Observation of the Singly Cabibbo-Suppressed Decay $D^+ \to \omega\pi^+$ and Evidence for $D^0 \to \omega\pi^0$

M. Ablikim[1], M. N. Achasov[9,f], X. C. Ai[1], O. Albayrak[5], M. Albrecht[4], D. J. Ambrose[44], A. Amoroso[49A,49C], F. F. An[1], Q. An[46,a], J. Z. Bai[1], R. Baldini Ferroli[20A], Y. Ban[31], D. W. Bennett[19], J. V. Bennett[5], M. Bertani[20A], D. Bettoni[21A], J. M. Bian[43], F. Bianchi[49A,49C], E. Boger[23,d], I. Boyko[23], R. A. Briere[5], H. Cai[51], X. Cai[1,a], O. Cakir[40A,b], A. Calcaterra[20A], G. F. Cao[1], S. A. Cetin[40B], J. F. Chang[1,a], G. Chelkov[23,d,e], G. Chen[1], H. S. Chen[1], H. Y. Chen[2], J. C. Chen[1], M. L. Chen[1,a], S. Chen[41], S. J. Chen[29], X. Chen[1,a], X. R. Chen[26], Y. B. Chen[1,a], H. P. Cheng[17], X. K. Chu[31], G. Cibinetto[21A], H. L. Dai[1,a], J. P. Dai[34], A. Dbeyssi[14], D. Dedovich[23], Z. Y. Deng[1], A. Denig[22], I. Denysenko[23], M. Destefanis[49A,49C], F. De Mori[49A,49C], Y. Ding[27], C. Dong[30], J. Dong[1,a], L. Y. Dong[1], M. Y. Dong[1,a], Z. L. Dou[29], S. X. Du[53], P. F. Duan[1], J. Z. Fan[39], J. Fang[1,a], S. S. Fang[1], X. Fang[46,a], Y. Fang[1], L. Fava[49B,49C], F. Feldbauer[22], G. Felici[20A], C. Q. Feng[46,a], E. Fioravanti[21A], M. Fritsch[14,22], C. D. Fu[1], Q. Gao[1], X. L. Gao[46,a], X. Y. Gao[2], Y. Gao[39], Z. Gao[46,a], I. Garzia[21A], K. Goetzen[10], W. X. Gong[1,a], W. Gradl[22], M. Greco[49A,49C], M. H. Gu[1,a], Y. T. Gu[12], Y. H. Guan[1], A. Q. Guo[1], L. B. Guo[28], R. P. Guo[1], Y. Guo[1], Y. P. Guo[22], Z. Haddadi[25], A. Hafner[22], S. Han[51], F. A. Harris[42], K. L. He[1], T. Held[4], Y. K. Heng[1,a], Z. L. Hou[1], C. Hu[28], H. M. Hu[1], J. F. Hu[49A,49C], T. Hu[1,a], Y. Hu[1], G. M. Huang[6], G. S. Huang[46,a], J. S. Huang[15], X. T. Huang[33], X. Z. Huang[29], Y. Huang[29], T. Hussain[48], Q. Ji[1], Q. P. Ji[30], X. B. Ji[1], X. L. Ji[1,a], L. W. Jiang[51], X. S. Jiang[1,a], X. Y. Jiang[30], J. B. Jiao[33], Z. Jiao[17], D. P. Jin[1,a], S. Jin[1], T. Johansson[50], A. Julin[43], N. Kalantar-Nayestanaki[25], X. L. Kang[1], X. S. Kang[30], M. Kavatsyuk[25], B. C. Ke[5], P. Kiese[22], R. Kliemt[14], B. Kloss[22], O. B. Kolcu[40B,i], B. Kopf[4], M. Kornicer[42], W. Kuehn[24], A. Kupsc[50], J. S. Lange[24], M. Lara[19], P. Larin[14], C. Leng[49C], C. Li[50], Cheng Li[46,a], D. M. Li[53], F. Li[1,a], F. Y. Li[31], G. Li[1], H. B. Li[1], H. J. Li[1], J. C. Li[1], Jin Li[32], K. Li[33], K. Li[13], Lei Li[3], P. R. Li[41], T. Li[33], W. D. Li[1], W. G. Li[1], X. L. Li[33], X. M. Li[12], X. N. Li[1,a], X. Q. Li[30], Z. B. Li[38], H. Liang[46,a], J. J. Liang[12], Y. F. Liang[36], Y. T. Liang[24], G. R. Liao[11], D. X. Lin[14], B. J. Liu[1], C. X. Liu[1], D. Liu[46,a], F. H. Liu[35], Fang Liu[1], Feng Liu[6], H. B. Liu[12], H. H. Liu[16], H. H. Liu[1], H. M. Liu[1], J. Liu[1], J. B. Liu[46,a], J. P. Liu[51], J. Y. Liu[1], K. Liu[39], K. Y. Liu[27], L. D. Liu[31], P. L. Liu[1,a], Q. Liu[41], S. B. Liu[46,a], X. Liu[26], Y. B. Liu[30], Z. A. Liu[1,a], Zhiqing Liu[22], H. Loehner[25], X. C. Lou[1,a,h], H. J. Lu[17], J. G. Lu[1,a], Y. Lu[1], Y. P. Lu[1,a], C. L. Luo[28], M. X. Luo[52], T. Luo[42], X. L. Luo[1,a], X. R. Lyu[41], F. C. Ma[27], H. L. Ma[1], L. L. Ma[33], M. M. Ma[1], Q. M. Ma[1], T. Ma[1], X. N. Ma[30], X. Y. Ma[1,a], F. E. Maas[14], M. Maggiora[49A,49C], Y. J. Mao[31], Z. P. Mao[1], S. Marcello[49A,49C], J. G. Messchendorp[25], J. Min[1,a], R. E. Mitchell[19], X. H. Mo[1,a], Y. J. Mo[6], C. Morales Morales[14], K. Moriya[19], N. Yu. Muchnoi[9,f], H. Muramatsu[43], Y. Nefedov[23], F. Nerling[14], I. B. Nikolaev[9,f], Z. Ning[1,a], S. Nisar[8], S. L. Niu[1,a], X. Y. Niu[1], S. L. Olsen[32], Q. Ouyang[1,a], S. Pacetti[20B], Y. Pan[46,a], P. Patteri[20A], M. Pelizaeus[4], H. P. Peng[46,a], K. Peters[10], J. Pettersson[50], J. L. Ping[28], R. G. Ping[1], R. Poling[43], V. Prasad[1], M. Qi[29], S. Qian[1,a], C. F. Qiao[41], L. Q. Qin[33], N. Qin[51], X. S. Qin[1], Z. H. Qin[1,a], J. F. Qiu[1], K. H. Rashid[48], C. F. Redmer[22], M. Ripka[22], G. Rong[1], Ch. Rosner[14], X. D. Ruan[12], A. Sarantsev[23,g], M. Savrié[21B], K. Schoenning[50], S. Schumann[22], W. Shan[31], M. Shao[46,a], C. P. Shen[2], P. X. Shen[30], X. Y. Shen[1], H. Y. Sheng[1], M. Shi[1], W. M. Song[1], X. Y. Song[1], S. Sosio[49A,49C], S. Spataro[49A,49C], G. X. Sun[1], J. F. Sun[15], S. S. Sun[1], X. H. Sun[1], Y. J. Sun[46,a], Y. Z. Sun[1], Z. J. Sun[1,a], Z. T. Sun[19], C. J. Tang[36], X. Tang[1], I. Tapan[40C], E. H. Thorndike[44], M. Tiemens[25], M. Ullrich[24], I. Uman[40B], G. S. Varner[42], B. Wang[30], B. L. Wang[41], D. Wang[31], D. Y. Wang[31], K. Wang[1,a], L. L. Wang[1], L. S. Wang[1], M. Wang[33], P. Wang[1], P. L. Wang[1], S. G. Wang[31], W. Wang[1,a], W. P. Wang[46,a], X. F. Wang[39], Y. Wang[37], Y. D. Wang[14], Y. F. Wang[1,a], Y. Q. Wang[22], Z. Wang[1,a], Z. G. Wang[1,a], Z. H. Wang[46,a], Z. Y. Wang[1], Z. Y. Wang[1], T. Weber[22], D. H. Wei[11], J. B. Wei[31], P. Weidenkaff[22], S. P. Wen[1], U. Wiedner[4], M. Wolke[50], L. H. Wu[1], L. J. Wu[1], Z. Wu[1,a], L. Xia[46,a], L. G. Xia[39], Y. Xia[18], D. Xiao[1], H. Xiao[47], Z. J. Xiao[28], Y. G. Xie[1,a], Q. L. Xiu[1,a], G. F. Xu[1], J. J. Xu[1], L. Xu[1], Q. J. Xu[13], X. P. Xu[37], L. Yan[49A,49C], W. B. Yan[46,a], W. C. Yan[46,a], Y. H. Yan[18], H. J. Yang[34], H. X. Yang[1], L. Yang[51], Y. Yang[6], Y. Y. Yang[11], M. Ye[1,a], M. H. Ye[7], J. H. Yin[1], B. X. Yu[1,a], C. X. Yu[30], J. S. Yu[26], C. Z. Yuan[1], W. L. Yuan[29], Y. Yuan[1], A. Yuncu[40B,c], A. A. Zafar[48], A. Zallo[20A], Y. Zeng[18], Z. Zeng[46,a], B. X. Zhang[1], B. Y. Zhang[1,a], C. Zhang[29], C. C. Zhang[1], D. H. Zhang[1], H. H. Zhang[38], H. Y. Zhang[1,a], J. Zhang[1], J. J. Zhang[1], J. L. Zhang[1], J. Q. Zhang[1], J. W. Zhang[1,a], J. Y. Zhang[1], J. Z. Zhang[1], K. Zhang[1], L. Zhang[1], X. Y. Zhang[33], Y. Zhang[1], Y. H. Zhang[1,a], Y. N. Zhang[41], Y. T. Zhang[46,a], Yu Zhang[41], Z. H. Zhang[6], Z. P. Zhang[46], Z. Y. Zhang[51], G. Zhao[1], J. W. Zhao[1,a], J. Y. Zhao[1], J. Z. Zhao[1,a], Lei Zhao[46,a], Ling Zhao[1], M. G. Zhao[30], Q. Zhao[1], Q. W. Zhao[1], S. J. Zhao[53], T. C. Zhao[1], Y. B. Zhao[1,a], Z. G. Zhao[46,a], A. Zhemchugov[23,d], B. Zheng[47], J. P. Zheng[1,a], W. J. Zheng[33], Y. H. Zheng[41], B. Zhong[28], L. Zhou[1,a], X. Zhou[51], X. K. Zhou[46,a], X. R. Zhou[46,a], X. Y. Zhou[1], K. Zhu[1], K. J. Zhu[1,a], S. Zhu[1], S. H. Zhu[45], X. L. Zhu[39], Y. C. Zhu[46,a], Y. S. Zhu[1], Z. A. Zhu[1], J. Zhuang[1,a], L. Zotti[49A,49C], B. S. Zou[1], J. H. Zou[1]

(BESIII Collaboration)

[1] *Institute of High Energy Physics, Beijing 100049, People's Republic of China*
[2] *Beihang University, Beijing 100191, People's Republic of China*
[3] *Beijing Institute of Petrochemical Technology, Beijing 102617, People's Republic of China*
[4] *Bochum Ruhr-University, D-44780 Bochum, Germany*
[5] *Carnegie Mellon University, Pittsburgh, Pennsylvania 15213, USA*
[6] *Central China Normal University, Wuhan 430079, People's Republic of China*
[7] *China Center of Advanced Science and Technology, Beijing 100190, People's Republic of China*
[8] *COMSATS Institute of Information Technology, Lahore, Defence Road, Off Raiwind Road, 54000 Lahore, Pakistan*
[9] *G.I. Budker Institute of Nuclear Physics SB RAS (BINP), Novosibirsk 630090, Russia*
[10] *GSI Helmholtzcentre for Heavy Ion Research GmbH, D-64291 Darmstadt, Germany*
[11] *Guangxi Normal University, Guilin 541004, People's Republic of China*
[12] *GuangXi University, Nanning 530004, People's Republic of China*
[13] *Hangzhou Normal University, Hangzhou 310036, People's Republic of China*
[14] *Helmholtz Institute Mainz, Johann-Joachim-Becher-Weg 45, D-55099 Mainz, Germany*
[15] *Henan Normal University, Xinxiang 453007, People's Republic of China*
[16] *Henan University of Science and Technology, Luoyang 471003, People's Republic of China*
[17] *Huangshan College, Huangshan 245000, People's Republic of China*

Typeset by REVTeX

^{18} *Hunan University, Changsha 410082, People's Republic of China*
^{19} *Indiana University, Bloomington, Indiana 47405, USA*
^{20} *(A)INFN Laboratori Nazionali di Frascati, I-00044, Frascati, Italy; (B)INFN and University of Perugia, I-06100, Perugia, Italy*
^{21} *(A)INFN Sezione di Ferrara, I-44122, Ferrara, Italy; (B)University of Ferrara, I-44122, Ferrara, Italy*
^{22} *Johannes Gutenberg University of Mainz, Johann-Joachim-Becher-Weg 45, D-55099 Mainz, Germany*
^{23} *Joint Institute for Nuclear Research, 141980 Dubna, Moscow region, Russia*
^{24} *Justus Liebig University Giessen, II. Physikalisches Institut, Heinrich-Buff-Ring 16, D-35392 Giessen, Germany*
^{25} *KVI-CART, University of Groningen, NL-9747 AA Groningen, The Netherlands*
^{26} *Lanzhou University, Lanzhou 730000, People's Republic of China*
^{27} *Liaoning University, Shenyang 110036, People's Republic of China*
^{28} *Nanjing Normal University, Nanjing 210023, People's Republic of China*
^{29} *Nanjing University, Nanjing 210093, People's Republic of China*
^{30} *Nankai University, Tianjin 300071, People's Republic of China*
^{31} *Peking University, Beijing 100871, People's Republic of China*
^{32} *Seoul National University, Seoul, 151-747 Korea*
^{33} *Shandong University, Jinan 250100, People's Republic of China*
^{34} *Shanghai Jiao Tong University, Shanghai 200240, People's Republic of China*
^{35} *Shanxi University, Taiyuan 030006, People's Republic of China*
^{36} *Sichuan University, Chengdu 610064, People's Republic of China*
^{37} *Soochow University, Suzhou 215006, People's Republic of China*
^{38} *Sun Yat-Sen University, Guangzhou 510275, People's Republic of China*
^{39} *Tsinghua University, Beijing 100084, People's Republic of China*
^{40} *(A)Istanbul Aydin University, 34295 Sefakoy, Istanbul, Turkey; (B)Istanbul Bilgi University, 34060 Eyup, Istanbul, Turkey; (C)Uludag University, 16059 Bursa, Turkey*
^{41} *University of Chinese Academy of Sciences, Beijing 100049, People's Republic of China*
^{42} *University of Hawaii, Honolulu, Hawaii 96822, USA*
^{43} *University of Minnesota, Minneapolis, Minnesota 55455, USA*
^{44} *University of Rochester, Rochester, New York 14627, USA*
^{45} *University of Science and Technology Liaoning, Anshan 114051, People's Republic of China*
^{46} *University of Science and Technology of China, Hefei 230026, People's Republic of China*
^{47} *University of South China, Hengyang 421001, People's Republic of China*
^{48} *University of the Punjab, Lahore-54590, Pakistan*
^{49} *(A)University of Turin, I-10125, Turin, Italy; (B)University of Eastern Piedmont, I-15121, Alessandria, Italy; (C)INFN, I-10125, Turin, Italy*
^{50} *Uppsala University, Box 516, SE-75120 Uppsala, Sweden*
^{51} *Wuhan University, Wuhan 430072, People's Republic of China*
^{52} *Zhejiang University, Hangzhou 310027, People's Republic of China*
^{53} *Zhengzhou University, Zhengzhou 450001, People's Republic of China*

^{a} *Also at State Key Laboratory of Particle Detection and Electronics, Beijing 100049, Hefei 230026, People's Republic of China*
^{b} *Also at Ankara University,06100 Tandogan, Ankara, Turkey*
^{c} *Also at Bogazici University, 34342 Istanbul, Turkey*
^{d} *Also at the Moscow Institute of Physics and Technology, Moscow 141700, Russia*
^{e} *Also at the Functional Electronics Laboratory, Tomsk State University, Tomsk, 634050, Russia*
^{f} *Also at the Novosibirsk State University, Novosibirsk, 630090, Russia*
^{g} *Also at the NRC "Kurchatov Institute, PNPI, 188300, Gatchina, Russia*
^{h} *Also at University of Texas at Dallas, Richardson, Texas 75083, USA*
^{i} *Also at Istanbul Arel University, 34295 Istanbul, Turkey*

Based on 2.93 fb^{-1} e^+e^- collision data taken at center-of-mass energy of 3.773 GeV by the BESIII detector, we report searches for the singly Cabibbo-suppressed decays $D^+ \to \omega\pi^+$ and $D^0 \to \omega\pi^0$. A double tag technique is used to measure the absolute branching fractions $\mathcal{B}(D^+ \to \omega\pi^+) = (2.79 \pm 0.57 \pm 0.16) \times 10^{-4}$ and $\mathcal{B}(D^0 \to \omega\pi^0) = (1.17 \pm 0.34 \pm 0.07) \times 10^{-4}$, with statistical significances of 5.5σ and 4.1σ, respectively. We also present measurements of the absolute branching fractions for the related $\eta\pi$ decay modes. We find $\mathcal{B}(D^+ \to \eta\pi^+) = (3.07 \pm 0.22 \pm 0.13) \times 10^{-3}$ and $\mathcal{B}(D^0 \to \eta\pi^0) = (0.65 \pm 0.09 \pm 0.04) \times 10^{-3}$, which are consistent with the current world averages. The first and second uncertainties are statistical and systematic, respectively.

Hadronic decays of charm mesons provide important in-put for beauty physics and also open a window into the study

of strong final state interactions. For Cabibbo-suppressed charm decays, precise measurements are challenging due to low statistics and high backgrounds. Among them, the singly Cabibbo-suppressed (SCS) decays $D^{+,0} \to \omega\pi^{+,0}$ have not yet been observed. The most recent experimental search was performed by the CLEO Collaboration in 2006 [1] with a 281 pb^{-1} data collected on the $\psi(3770)$ peak. The branching ratio upper limits were set to be 3.4×10^{-4} and 2.6×10^{-4} at the 90% confidence level (C.L.) for $D^+ \to \omega\pi^+$ and $D^0 \to \omega\pi^0$, respectively [1]. Following the diagrammatic approach, the small decay rates may be caused by the destructive interference between the color-suppressed quark diagrams C_V and C_P [2]. Numerically, if W-annihilation contributions are neglected, the branching fractions of the $D \to \omega\pi$ decays should be at about 1.0×10^{-4} level [2, 3].

Besides searching for $D^{+,0} \to \omega\pi^{+,0}$, we also report measurements of the branching fractions for the decays $D^{+,0} \to \eta\pi^{+,0}$. Precise measurements of these decay rates can improve understanding of U-spin and $SU(3)$-flavor symmetry breaking effects in D decays, benefiting theoretical predictions of CP violation in D decays [4].

We employ the "double tag" (DT) technique first developed by the MARK-III Collaboration [5, 6] to perform absolute measurements of the branching fractions. As the peak of the $\psi(3770)$ resonance is just above the $D\bar{D}$ threshold and below the $D\bar{D}\pi$ threshold, for D meson we are interested, only $D\bar{D}$ pair-production is allowed. We select "single tag" (ST) events in which either a D or $\bar{D}$ is fully reconstructed without reference to the other meson. We then look for the D decays of interest in the remainder of each event, namely, in DT events where both the D and $\bar{D}$ are fully reconstructed. This strategy suppresses background and provides an absolute normalization for branching fraction measurements without the need for knowledge of the luminosity or the $e^+e^- \to D\bar{D}$ production cross section. The absolute branching fractions for D meson decays are calculated by the general formula

$$\mathcal{B}_{\text{sig}} = \frac{\sum_\alpha N_{\text{sig}}^{\text{obs},\alpha}}{\sum_\alpha N_{\text{tag}}^{\text{obs},\alpha} \epsilon_{\text{tag,sig}}^{\alpha}/\epsilon_{\text{tag}}^{\alpha}}, \quad (1)$$

where α denotes different ST modes, $N_{\text{tag}}^{\text{obs},\alpha}$ is the yield of ST events for the tag mode α, $N_{\text{sig}}^{\text{obs},\alpha}$ is the corresponding yield of DT events, and $\epsilon_{\text{tag}}^{\alpha}$ and $\epsilon_{\text{tag,sig}}^{\alpha}$ are the ST and DT efficiencies for the tag mode α.

BESIII is a general-purpose magnetic spectrometer with a helium-gas-based drift chamber (MDC), a plastic scintillator time-of-flight system (TOF), and a CsI(Tl) electromagnetic calorimeter (EMC) enclosed in a superconducting solenoidal magnet providing a 1.0 T field. The solenoid is supported by an octagonal flux-return yoke with resistive-plate counters interleaved with steel for muon identification (MUC). The acceptance for charged particles and photons is 93% of 4π, and the charged particle momentum and barrel (endcap) photon energy resolutions at 1 GeV are 0.5% and 2.5% (5.0%), respectively [7]. The data used has an integrated luminosity of 2.93 fb^{-1} [8] and was collected with the BESIII detector at a center-of-mass energy of 3.773 GeV.

A GEANT4-based [9] Monte-Carlo (MC) simulation package, which includes the geometric description of the detector and the detector response, is used to determine the detection efficiency and to estimate the potential peaking background. Signal MC samples of a D meson decaying only to $\omega\pi$ ($\eta\pi$) together with a $\bar{D}$ decaying only to the tag modes used are generated by the MC generator KKMC [10] using EVTGEN [11], with initial state radiation (ISR) effects [12] and final state radiation effects [13] included. For the background studies, MC samples of $\psi(3770) \to D^0\bar{D}^0, D^+D^-$ and $\psi(3770) \to$ non-$D\bar{D}$ decays, ISR production of $\psi(3686)$ and J/ψ, and $e^+e^- \to q\bar{q}$ continuum processes, are produced at $\sqrt{s} = 3.773$ GeV. All known decay modes of the various D and ψ mesons are generated with branching fractions taken from the Particle Data Group (PDG) [14], and the remaining decays are generated with LUNDCHARM [15].

Charged tracks are required to be well-measured and to satisfy criteria based on the track fit quality; the angular range is restricted to $|\cos\theta| < 0.93$, where θ is the polar angle with respect to the direction of positron beam. Tracks (except for K_S^0 daughters) must also be consistent with coming from the interaction point (IP) in three dimensions. Particle identification (PID) combining information of measured energy loss (dE/dx) in the MDC and the flight time obtained from the TOF is used to separate charged kaons and pions, the likelihood is required to be $\mathcal{L}(K) > \mathcal{L}(\pi)$, $\mathcal{L}(K) > 0$ for kaons and vice-versa for pions. Electromagnetic showers are reconstructed by clustering EMC crystal energies; efficiency and energy resolution are improved by including the energy deposited in nearby TOF counters. To identify photon candidates, showers must have minimum energies of 25 MeV for $|\cos\theta| < 0.80$ (barrel region) or 50 MeV for $0.86 < |\cos\theta| < 0.92$ (endcap regions). The angle between the shower direction and all track extrapolations to the EMC must be larger than 10 standard deviations. A requirement on the EMC timing suppresses electronic noise and energy deposits unrelated to the event. The π^0 candidates are reconstructed by requiring the diphoton invariant mass to obey $M_{\gamma\gamma} \in (0.115, 0.150)$ GeV/c^2. Candidates with both photons coming from the endcap regions are rejected due to poor resolution. To improve resolution and reduce background, we constrain the invariant mass of each photon pair to the nominal π^0 mass [14]. The K_S^0 candidates are selected from pairs of oppositely charged and vertex-constrained tracks consistent with coming from the IP along the beam direction but free of aforementioned PID and having an invariant mass in the range $0.487 < M_{\pi^+\pi^-} < 0.511$ GeV/c^2.

The ST candidate events are selected by reconstructing a D^- or $\bar{D}^0$ in the following hadronic final states: $D^- \to K^+\pi^-\pi^-$, $K^+\pi^-\pi^-\pi^0$, $K_S^0\pi^-$, $K_S^0\pi^-\pi^0$, $K_S^0\pi^+\pi^-\pi^-$, $K^+K^-\pi^-$, and $\bar{D}^0 \to K^+\pi^-$, $K^+\pi^-\pi^0$, $K^+\pi^-\pi^+\pi^-$, $K^+\pi^-\pi^0\pi^0$, $K^+\pi^-\pi^+\pi^-\pi^0$, comprising approximately 28.0% and 38.0% [14] of all D^- and $\bar{D}^0$ decays, respectively. For the signal side, we reconstruct $D^+ \to \omega\pi^+(\eta\pi^+)$ and $D^0 \to \omega\pi^0(\eta\pi^0)$, with $\omega(\eta) \to \pi^+\pi^-\pi^0$. Throughout the paper, charge-conjugate modes are implicitly implied, unless otherwise noted.

To identify the reconstructed D candidates, we use two

variables, the beam-constrained mass, M_{BC}, and the energy difference, ΔE, which are defined as

$$M_{BC} \equiv \sqrt{E_{beam}^2/c^4 - |\vec{p}_D|^2/c^2}, \ \Delta E \equiv E_D - E_{beam}. \quad (2)$$

Here, $\vec{p}_D$ and E_D are the reconstructed momentum and energy of the D candidate in the e^+e^- center-of-mass system, and E_{beam} is the beam energy. For true $D^{+,0}$ candidates, ΔE will be consistent with zero, and M_{BC} consistent with the $D^{+,0}$ mass. The resolution of M_{BC} is less than 2 MeV/c^2 and is dominated by the beam energy spread. The ΔE resolution is about 10 MeV for final states consisting entirely of charged tracks, but increases to about 15 (20) MeV for cases where one (two) π^0 are included. We accept D candidates with M_{BC} greater than 1.83 GeV/c^2 and with mode-dependent ΔE requirements of approximately three standard deviations (σ) around the fitted double Gaussian means. For the ST modes, we accept at most one candidate per mode per event; the candidate with the smallest $|\Delta E|$ is chosen [16].

To obtain ST yields, we fit the M_{BC} distributions of the accepted D candidates, as shown in Fig. 1. The signal shape which is modeled by MC shape convoluted with a Gaussian function includes the effects of beam energy spread, ISR, the $\psi(3770)$ line shape, and resolution. Combinatorial background is modeled by an ARGUS function [17]. With requirement of $1.866 < M_{BC}^{tag} < 1.874$ GeV/c^2 for D^+ case or $1.859 < M_{BC}^{tag} < 1.871$ GeV/c^2 for D^0 case, ST yields are calculated by subtracting the integrated ARGUS background yields within the signal region from the total event counts in this region. The tag efficiency is studied using MC samples following the same procedure. The ST yields in data and corresponding tag efficiencies are listed in Table I.

On the signal side we search for $D^+ \to \pi^+\pi^-\pi^0\pi^+$ and $D^0 \to \pi^+\pi^-\pi^0\pi^0$ modes containing an $\omega(\eta) \to \pi^+\pi^-\pi^0$ decay. The requirements on ΔE are applied similar as in the tag selection; if multiple candidates are found, the candidate with the minimum $|\Delta E|$ is chosen. For both D^+ and D^0 decays, two possible ω (η) combinations exist. Combinations with 3π mass in the interval $(0.4, 1.0)$ GeV/c^2 are considered. The chance that both ω (η) candidates combinations lie in this region is only about 0.3%, rendering this source of multiple candidates negligible.

With the DT technique, the continuum background $e^+e^- \to q\bar{q}$ is highly suppressed. The remaining background dominantly comes from $D\bar{D}$ events broadly populating the 3π mass window. To suppress the non-ω background, we require that the helicity, $H_\omega \equiv \cos\theta_H$, of the ω have an absolute value larger than 0.54 (0.51) for D^+ (D^0). The angle θ_H is the opening angle between the direction of the normal to the $\omega \to 3\pi$ decay plane and direction of the D meson in the ω rest frame. True ω signal from D decays is longitudinally polarized so we expect a $\cos^2\theta_H \equiv H_\omega^2$ distribution. To further suppress background from $D^{+,0} \to K_S^0\pi^{+\pi^0,-}$ with $K_S^0 \to \pi^+\pi^-$, we apply a K_S^0 veto by requiring $|M_{\pi^+\pi^-} - m_{K_S^0}^{PDG}| > 12$ (9) MeV/c^2 for the D^+ (D^0) analysis. Here, $m_{K_S^0}^{PDG}$ is the known K_S^0 mass and $M_{\pi^+\pi^-}$ is calculated at the IP for simplicity. The requirements on the ω helicity and K_S^0 veto are optimized to get max-
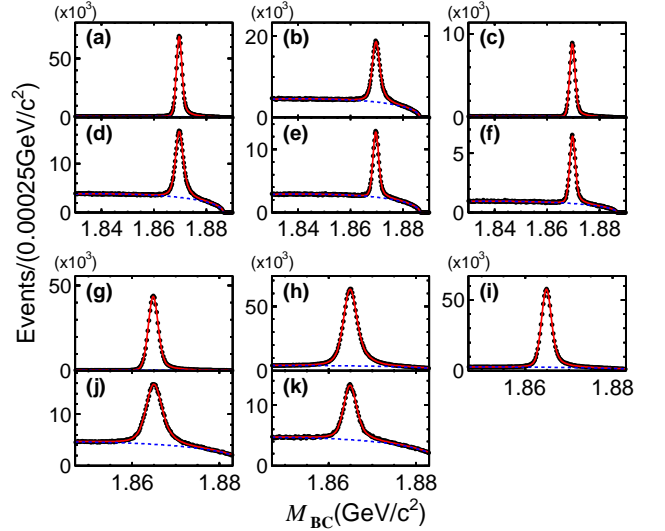

FIG. 1. M_{BC} distributions of ST samples for different tag modes. The first two rows show charged D decays: (a) $K^+\pi^-\pi^-$, (b) $K^+\pi^-\pi^-\pi^0$, (c) $K_S^0\pi^-$, (d) $K_S^0\pi^-\pi^0$, (e) $K_S^0\pi^+\pi^-\pi^-$, (f) $K^+K^-\pi^-$, the latter two rows show neutral D decays: (g) $K^+\pi^-$, (h) $K^+\pi^-\pi^0$, (i) $K^+\pi^-\pi^+\pi^-$, (j) $K^+\pi^-\pi^0\pi^0$, (k) $K^+\pi^-\pi^+\pi^-\pi^0$. Data are shown as points, the (red) solid lines are the total fits and the (blue) dashed lines are the background shapes. D and $\bar{D}$ candidates are combined.

imum sensitivity based on the signal MC events and data in ω sidebands.

After the above selection criteria, the signal region **S** for the DT candidates is defined as $1.866 < M_{BC} < 1.874$ GeV/c^2 for the D^+ ($1.859 < M_{BC} < 1.871$ GeV/c^2 for the D^0) in the two-dimensional (2D) M_{BC}^{sig} versus M_{BC}^{tag} plane, as illustrated in Fig. 2. We also define sideband box regions to estimate potential background [18]. Sidebands **A** and **B** contain candidates where either the D or the $\bar{D}$ is misreconstructed. Sidebands **C** and **D** contain candidates where both D and $\bar{D}$ are misreconstructed, either in a correlated way (**C**), by assigning daughter particles to the wrong parent, or in an uncorrelated way (**D**).
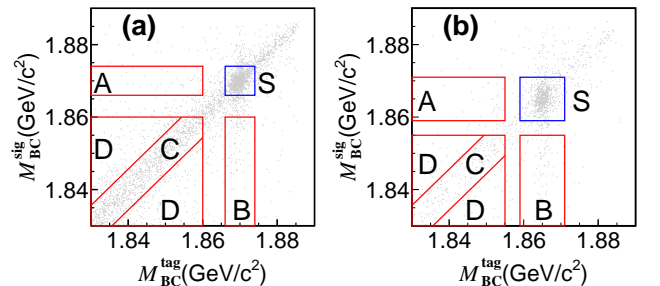

FIG. 2. 2D M_{BC} distributions for (a) $D^+ \to \omega\pi^+$ and (b) $D^0 \to \omega\pi^0$ with the signal (**S**) and sideband (**A, B, C, D**) regions used for background estimation indicated.

TABLE I. ST data yields ($N_{\mathrm{tag}}^{\mathrm{obs}}$), ST ($\epsilon_{\mathrm{tag}}$) and DT ($\epsilon_{\mathrm{tag,sig}}^{\omega}$ and $\epsilon_{\mathrm{tag,sig}}^{\eta}$) efficiencies, and their statistical uncertainties. Branching fractions of the K_S^0 and π^0 are not included in the efficiencies, but are included in the branching fraction calculations. The first six rows are for D^- and the last five are for $\bar{D}^0$.

| Mode	ST Yields	ϵ_{tag} (%)	$\epsilon_{\mathrm{tag,sig}}^{\omega}$(%)	$\epsilon_{\mathrm{tag,sig}}^{\eta}$(%)
$K^+\pi^-\pi^-$	772711 ± 895	48.76 ± 0.02	11.01 ± 0.15	12.64 ± 0.17
$K^+\pi^-\pi^-\pi^0$	226969 ± 608	23.19 ± 0.02	4.47 ± 0.10	5.26 ± 0.11
$K_S^0\pi^-$	95974 ± 315	52.35 ± 0.07	11.69 ± 0.18	13.99 ± 0.21
$K_S^0\pi^-\pi^0$	211872 ± 572	26.68 ± 0.03	5.35 ± 0.13	6.44 ± 0.14
$K_S^0\pi^-\pi^+\pi^-$	121801 ± 459	30.53 ± 0.04	6.16 ± 0.13	7.17 ± 0.15
$K^+K^-\pi^-$	65955 ± 306	38.72 ± 0.07	8.50 ± 0.13	9.76 ± 0.14
$K^+\pi^-$	529558 ± 745	64.79 ± 0.03	12.44 ± 0.16	14.17 ± 0.17
$K^+\pi^-\pi^0$	1044963 ± 1164	34.13 ± 0.01	5.73 ± 0.11	6.87 ± 0.12
$K^+\pi^-\pi^+\pi^-$	708523 ± 946	38.33 ± 0.02	6.04 ± 0.11	7.00 ± 0.13
$K^+\pi^-\pi^0\pi^0$	236719 ± 747	13.87 ± 0.02	1.78 ± 0.06	2.10 ± 0.07
$K^+\pi^-\pi^+\pi^-\pi^0$	152025 ± 684	15.55 ± 0.03	1.93 ± 0.06	2.08 ± 0.07
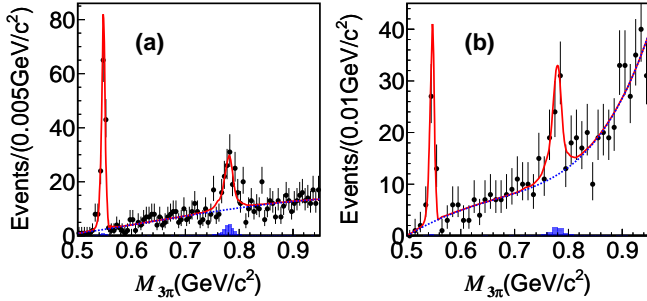
FIG. 3. Fits to the 3π mass spectra for (a) $D^+ \to \pi^+\pi^-\pi^0\pi^+$ and (b) $D^0 \to \pi^+\pi^-\pi^0\pi^0$ in the signal region **S** as defined in Fig. 2. Points are data; the (red) solid lines are the total fits; the (blue) dashed lines are the background shapes, and the hatched histograms are peaking background estimated from 2D M_{BC} sidebands.

To obtain the $\omega(\eta)$ yield, we perform a fit to the $\pi^+\pi^-\pi^0$ invariant mass ($M_{3\pi}$) distribution with events in the signal region **S**. The $\omega(\eta)$ shape is modeled by the signal MC shape convoluted with a Gaussian function to describe the difference in the $M_{3\pi}$ resolution between MC and data. Due to high statistics, the width σ_η of the Gaussian for the η case is determined by the fit, while the width σ_ω for the ω case is constrained by the MC-determined ratio $R = \sigma_\omega^{\mathrm{MC}}/\sigma_\eta^{\mathrm{MC}}$ giving the relative $M_{3\pi}$ resolution for η and ω final states. For D^+, the background shape is described by a third-order Chebychev polynomial, while for D^0 we use a shape of $a_0 M_{3\pi}^{1/2} + a_1 M_{3\pi}^{3/2} + a_2 M_{3\pi}^{5/2} + a_3 M_{3\pi}^{7/2} + a_4 M_{3\pi}^{9/2}$, where a_i ($i = 0, \ldots, 4$) are free parameters. The fit results are shown in Fig. 3, and the total ω yields N_ω for D^+ and D^0 cases are listed in Table II.

To estimate the $\omega(\eta)$ yield in the signal region **S** from background processes, event counts in sidebands **A**, **B**, and **C** are projected into the signal region **S** using scale factors deter-
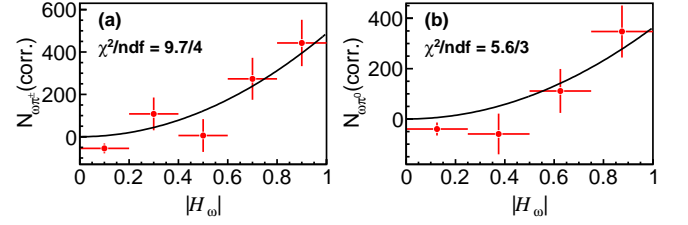

FIG. 4. Efficiency corrected yields versus $|H_\omega|$ for (a) $D^+ \to \omega\pi^+$ and (b) $D^0 \to \omega\pi^0$. Both are consistent with a distribution like $\cos^2\theta_H$ (black line).

mined from integrating the background shape in the ST M_{BC} fits. Contributions to sideband **D** are assumed to be uniformly distributed across the other regions [18]. For these events from the sideband regions, we perform similar fits to the 3π mass spectra, and find the peaking background yields $N_{\omega(\eta)}^{\mathrm{bkg}}$ for D^+ and D^0 respectively, as listed in Table II. By subtracting the ω peaking background extending underneath the signal region, the DT signal yields, $N_{\mathrm{sig}}^{\mathrm{obs}}$, are obtained. The statistical significances for $D^+ \to \omega\pi^+$ and $D^0 \to \omega\pi^0$ are found to be 5.5σ and 4.1σ, respectively, as determined by the ratio of the nominal maximum likelihood value and the likelihood value for a fit where the signal is set to zero by fixing the total yield N_ω to be equal to the sideband based background prediction, $N_{\omega(\eta)}^{\mathrm{bkg}}$.

TABLE II. Summary for the total $\omega(\eta)$ yields ($N_{\omega(\eta)}$), $\omega(\eta)$ peaking background yields ($N_{\omega(\eta)}^{\mathrm{bkg}}$) and net DT yields ($N_{\mathrm{sig}}^{\mathrm{obs}}$) in the signal region **S** as defined in Fig. 2. $N_{\mathrm{sig}}^{\mathrm{obs}}$ is estimated from the defined sidebands. The errors are statistical.

Mode	$N_{\omega(\eta)}$	$N_{\omega(\eta)}^{\mathrm{bkg}}$	$N_{\mathrm{sig}}^{\mathrm{obs}}$
$D^+ \to \omega\pi^+$	100 ± 16	21 ± 4	79 ± 16
$D^0 \to \omega\pi^0$	50 ± 12	5 ± 5	45 ± 13
$D^+ \to \eta\pi^+$	264 ± 17	6 ± 2	258 ± 18
$D^0 \to \eta\pi^0$	78 ± 10	3 ± 2	75 ± 10

We now remove the ω helicity requirement, and investigate the helicity dependence of our signal yields. By following procedures similar to those described above, we obtain the signal yield in each $|H_\omega|$ bin. The efficiency corrected yields are shown in Fig. 4, demonstrating agreement with expected $\cos^2\theta_H$ behavior, further validating this analysis.

With analogous selection criteria, we also determine $\mathcal{B}(D^{+,0} \to \eta\pi^{+,0})$ as a cross-check. The results are found to be consistent with the nominal results given below for $\mathcal{B}(D^{+,0} \to \eta\pi^{+,0})$, using relaxed cuts, as well as the PDG listings [14].

As shown in Fig. 3, the background level in the η signal region of the 3π invariant mass distribution is small compared to that near the ω mass. Also, according to the MC simula-
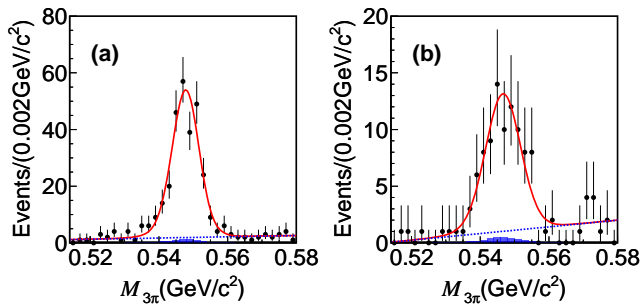
FIG. 5. Fits to the 3π mass spectra for (a) $D^+ \to \pi^+\pi^-\pi^0\pi^+$ and (b) $D^0 \to \pi^+\pi^-\pi^0\pi^0$ in the η mass region for the signal region **S** as defined in Fig. 2. Points are data; the (red) solid lines are the total fits; the (blue) dashed lines are the background shapes, and the hatched histograms are peaking background estimated from 2D M_{BC} sidebands.

tions and fits to events from the 2D M_{BC} sideband regions, η peaking background is small, as shown in Fig. 3. Therefore, to improve statistics, we remove the K_S^0 veto requirements and also make no helicity requirement since $H_\eta \equiv \cos\theta_H$ for signal is flat. Following a similar fit procedure, with results shown in Fig. 5, we determine $\eta\pi^+$ and $\eta\pi^0$ DT yields as listed in Table II.

With the DT technique, the branching fraction measurements are insensitive to systematics coming from the ST side since they mostly cancel. For the signal side, systematic uncertainties mainly come from imperfect knowledge of the efficiencies for tracking finding, PID criteria, the K_S^0 veto, and the H_ω requirement; additional uncertainties are related to the fit procedures.

Possible differences in tracking, PID and π^0 reconstruction efficiencies between data and the MC simulations are investigated using a partial-reconstruction technique based on the control samples $D^0 \to K^-\pi^+\pi^0$ and $D^0 \to K^-\pi^+$. We assign uncertainties of 1.0% and 0.5% per track for track finding and PID, respectively, and 1.0% per reconstructed π^0.

Uncertainty due to the 2D signal region definition is investigated via the relative change in signal yields for different signal region definitions based on the control samples $D^+ \to K_S^0\pi^+\pi^0$ and $D^0 \to K_S^0\pi^0\pi^0$ which have the same pions in the final state as our signal modes. With the same control samples, uncertainties due to the ΔE requirements are also studied. The relative data-MC efficiency differences are taken as systematic uncertainties, as listed in Table III.

Uncertainty due to the $|H_\omega|$ requirement is studied using the control sample $D^0 \to K_S^0\omega$. The data-MC efficiency difference with or without this requirement is taken as our systematic. Uncertainty due to the K_S^0 veto is similarly obtained with this control sample.

The ω peaking background is estimated from 2D M_{BC} sidebands. We change the sideband ranges by 2 MeV/c^2 for both sides and investigate the fluctuation on the signal yields, which is taken as a systematic uncertainty.

In the nominal fit to the $M_{3\pi}$ distribution, the ratio R, which is the relative difference on the $M_{3\pi}$ resolution between η and

ω positions, is determined by MC simulations. With control samples $D^0 \to K_S^0\eta$ and $K_S^0\omega$, the difference between data and MC defined as $\delta R = R_{\text{data}}/R_{\text{MC}} - 1$ is obtained. We vary the nominal R value by $\pm 1\sigma$ and take the relative change of signal yields as a systematic uncertainty.

Uncertainties due to the background shapes are investigated by changing the orders of the polynomials employed. Uncertainties due to the $M_{3\pi}$ fitting range are investigated by changing the range from $(0.50, 0.95)$ GeV/c^2 to $(0.48, 0.97)$ GeV/c^2 in the fits, yielding relative differences which are taken as systematic uncertainties.

We summarize the systematic uncertainties in Table III. The total effect is calculated by combining the uncertainties from all sources in quadrature.

TABLE III. Summary of systematic uncertainties in %. Uncertainties which are not involved are denoted by "–".

Source	$\omega\pi^+$	$\omega\pi^0$	$\eta\pi^+$	$\eta\pi^0$
$\pi^\pm$ tracking	3.0	2.0	3.0	2.0
$\pi^\pm$ PID	1.5	1.0	1.5	1.0
π^0 reconstruction	1.0	2.0	1.0	2.0
2D M_{BC} window	0.1	0.2	0.1	0.2
ΔE requirement	0.5	1.6	0.5	1.6
$|H_\omega|$ requirement	3.4	3.4	–	–
K_S^0 veto	0.8	0.8	–	–
Sideband regions	1.3	2.2	0.0	0.5
Signal resolution	0.9	0.9	–	–
Background shape	2.3	1.3	1.9	3.5
Fit range	0.3	1.9	0.8	1.5
$\mathcal{B}(\omega(\eta) \to \pi^+\pi^-\pi^0)$ [14]	0.8	0.8	1.2	1.2
Overall	5.8	6.0	4.3	5.3

Finally, the measured branching fractions of $D \to \omega\pi$ and $\eta\pi$ are summarized in Table IV, where the first errors are statistical and the second ones are systematic.

TABLE IV. Summary of branching fraction measurements, and comparison with the previous measurements for $D \to \omega\pi$ [1] and $D \to \eta\pi$ [19].

Mode	This work	Previous measurements
$D^+ \to \omega\pi^+$	$(2.79 \pm 0.57 \pm 0.16) \times 10^{-4}$	$< 3.4 \times 10^{-4}$ at 90% C.L.
$D^0 \to \omega\pi^0$	$(1.17 \pm 0.34 \pm 0.07) \times 10^{-4}$	$< 2.6 \times 10^{-4}$ at 90% C.L.
$D^+ \to \eta\pi^+$	$(3.07 \pm 0.22 \pm 0.13) \times 10^{-3}$	$(3.53 \pm 0.21) \times 10^{-3}$
$D^0 \to \eta\pi^0$	$(0.65 \pm 0.09 \pm 0.04) \times 10^{-3}$	$(0.68 \pm 0.07) \times 10^{-3}$

In summary, we present the first observation of the SCS decay $D^+ \to \omega\pi^+$ with statistical significance of 5.5σ. We find the first evidence for the SCS decay $D^0 \to \omega\pi^0$ with statistical significance of 4.1σ. The results are consistent with the theoretical prediction [2], and can improve understanding of U-spin and $SU(3)$-flavor symmetry breaking effects in D decays [4]. We also present measurements of the branching

fractions for $D^+ \to \eta\pi^+$ and $D^0 \to \eta\pi^0$ which are consistent with the previous measurements [19].

[1] P. Rubin *et al.* [CLEO Collaboration], Phys. Rev. Lett. **96**, 081802 (2006).

[2] H. Y. Cheng and C. W. Chiang, Phys. Rev. D **81**, 074021 (2010).

[3] Hai-Yang Cheng, private communication.

[4] W. Kwong and S. P. Rosen, Phys. Lett. B **298**, 413 (1993); Y. Grossman and D. J. Robinson, JHEP **1304**, 067 (2013).

[5] R. M. Baltrusaitis *et al.* [MARK-III Collaboration], Phys. Rev. Lett. **56**, 2140 (1986).

[6] J. Adler *et al.* [MARK-III Collaboration], Phys. Rev. Lett. **60**, 89 (1988).

[7] M. Ablikim *et al.* [BESIII Collaboration], Nucl. Instrum. Meth. A **614**, 345 (2010).

[8] M. Ablikim *et al.* [BESIII Collaboration], Chin. Phys. C **37**, 123001 (2013); M. Ablikim *et al.* [BESIII Collaboration], arXiv:1507.08188 (accepted by Phys. Lett. B).

[9] S. Agostinelli *et al.* [GEANT4 Collaboration], Nucl. Instrum. Meth. A **506**, 250 (2003).

[10] S. Jadach, B. F. L. Ward and Z. Was, Comput. Phys. Commun. **130**, 260 (2000); Phys. Rev. D **63**, 113009 (2001).

[11] D. J. Lange, Nucl. Instrum. Meth. A **462**, 152 (2001); R. G. Ping, Chin. Phys. C **32**, 599 (2008).

[12] E. A. Kuraev and V. S. Fadin, Sov. J. Nucl. Phys. **41**, 466 (1985) [Yad. Fiz. **41**, 733 (1985)].

[13] E. Richter-Was, Phys. Lett. B **303**, 163 (1993).

[14] K. Nakamura *et al*. [Particle Data Group], J. Phys. G **37**, 075021 (2010) and 2011 partial update for the 2012 edition.

[15] J. C. Chen, G. S. Huang, X. R. Qi, D. H. Zhang and Y. S. Zhu, Phys. Rev. D **62**, 034003 (2000).

[16] Q. He *et al.* [CLEO Collaboration], Phys. Rev. Lett. **95**, 121801 (2005).

[17] H. Albrecht *et al.* [ARGUS Collaboration], Phys. Lett. B **241**, 278 (1990).

[18] D. M. Asner *et al.* [CLEO Collaboration], Phys. Rev. D **78**, 012001 (2008).

[19] H. Mendez *et al.* [CLEO Collaboration], Phys. Rev. D **81**, 052013 (2010).